

pubs.acs.org/crystal Article

# Understanding the Role of Bulky Side Chains on Polymorphism of BTBT-Based Organic Semiconductors

Hyunjoong Chung, Shanwen Chen, Bijal Patel, Guillaume Garbay, Yves H. Geerts, and Ying Diao\*



Cite This: Cryst. Growth Des. 2020, 20, 1646–1654



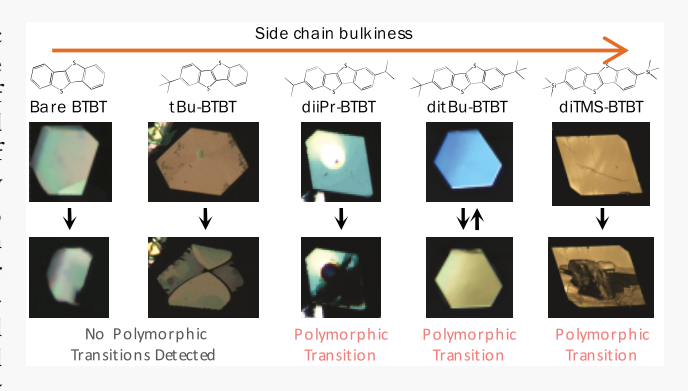
**ACCESS** 

Metrics & More

Article Recommendations

Supporting Information

ABSTRACT: Polymorphism plays a major role in organic electronics, since even the slightest change in packing can modulate electronic properties. Controlling and accessing polymorphs of organic semiconductors are critical, but they are usually discovered by serendipity. A clear understanding of the molecular origin of polymorphism is essential, but system-specific studies are largely prevalent, each system presenting a unique challenge. In this work, we conduct a systematic study of five organic semiconductors with the absence or presence of various bulky side chains. We discover polymorphs only in three out of five systems in their bulk single-crystal forms. The three systems that exhibit polymorphism all contain side chains on both ends of the core. We resolve the crystal structures and analyze key parameters for changes in the packing



environment such as density, intermolecular distance, and short contacts. These parameters indicate that the added bulky side chains loosen the molecular packing and that, as the side chains get bulkier, the effect is stronger. Thus, the bulky side chains create a packing environment more favorable for polymorphism. This proposes a generalizable molecular design rule for triggering polymorphs in organic semiconductors.

## ■ INTRODUCTION

The use of small molecules in organic electronics has become widely popular, fueled by their molecular versatility and solution processability. However, one critical challenge is polymorphism, which is the ability for a compound to adopt different crystalline packing states. Since even the slightest packing changes affect the electronic coupling and thus the charge transport,<sup>2-4</sup> polymorphism has a significant effect on the electronic performance. Therefore, polymorphism can severely impact device-to-device reproducibility, hampering the commercialization of organic electronics. A wide variety of high-performing systems experience polymorphism, including 6,13-bis(triisopropylsilylethynyl)pentacene (TIPS-penta-5,11-bis(triethylsilylethynyl)anthradithiophene (TES-ADT) derivatives,  $^{9,10}$  rubrene,  $^{11,12}$  N, N'-bis-(heptafluorobutyl)-2,6-dichloro-1,4,5,8-naphthalenetetracarboxylic diimide (Cl<sub>2</sub>-NDI), <sup>13</sup> and dithiophene-tetrathiafulvalene (DT-TTF).14

Polymorphism can also be a positive functional property<sup>15</sup> rather than a drawback, with its ability to enhance charge mobility by orders of magnitude. In this aspect, a variety of processing methods of accessing polymorphs with higher performance have been developed, a few of which are heating, <sup>1,6,9,16–18</sup> nanoconfinement, <sup>7</sup> solvent vapor annealing, <sup>13,16–18</sup> and solution shearing. <sup>7,19–21</sup> However, the focus of these studies is to develop methods that can access polymorphs of higher electronic performance, and they are not

aimed at a molecular-level understanding of why polymorphism occurs. Moreover, polymorphs are often discovered by serendipity, and thus each system presents a unique challenge. Whether polymorphism is a major hurdle to overcome or a promising functional property to exploit, a better understanding of the molecular origin of polymorphism is required for controlling polymorph formation.

In our work, we conduct a systematic study on a series of organic semiconductor systems  $^{22,23}$  with slight changes in the molecular structure to investigate the molecular origin of polymorphism. We vary the bulkiness of the side chains tethered on a common conjugated core, [1]benzothieno[3,2-b]benzothiophene (BTBT), and observe the polymorphic phase space. Interestingly, we discovered that, under the extensive set of conditions tested for in this work, three systems that contain side chains on both ends of the core show polymorphic behavior, whereas the two systems that have no side chains or a single side chain do not have polymorphs. We study the changes in the molecular structure that arise from adding various bulky side chains to understand the role of side chains on polymorphism.

Received: October 14, 2019 Revised: February 10, 2020 Published: February 11, 2020



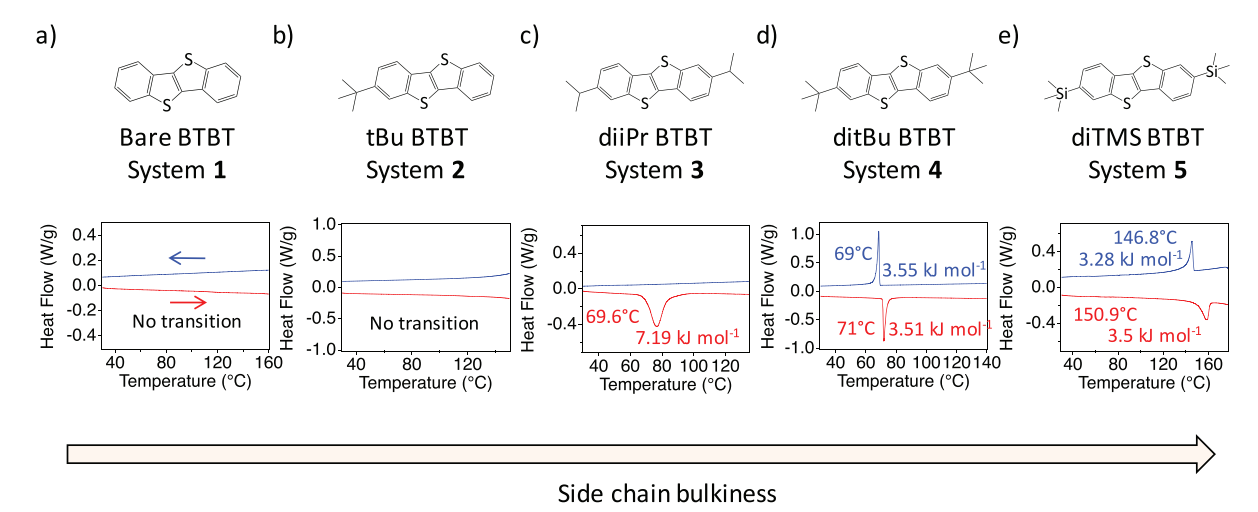


Figure 1. DSC results of five BTBT systems of increasing side chain bulkiness. Molecular structures and DSC results of systems 1-5 are shown in (a)-(e), respectively. The structures show increasing side chain bulkiness. The DSC results show solid-state polymorph transitions in three out of five systems. Red curves indicate data taken during heating, and blue curves indicate data taken during cooling at a rate of  $10\,^{\circ}$ C min $^{-1}$ . Downward peaks indicate endothermic transitions. Onset transition temperatures and enthalpy values for heating and/or cooling are indicated on the DSC graph for each system.

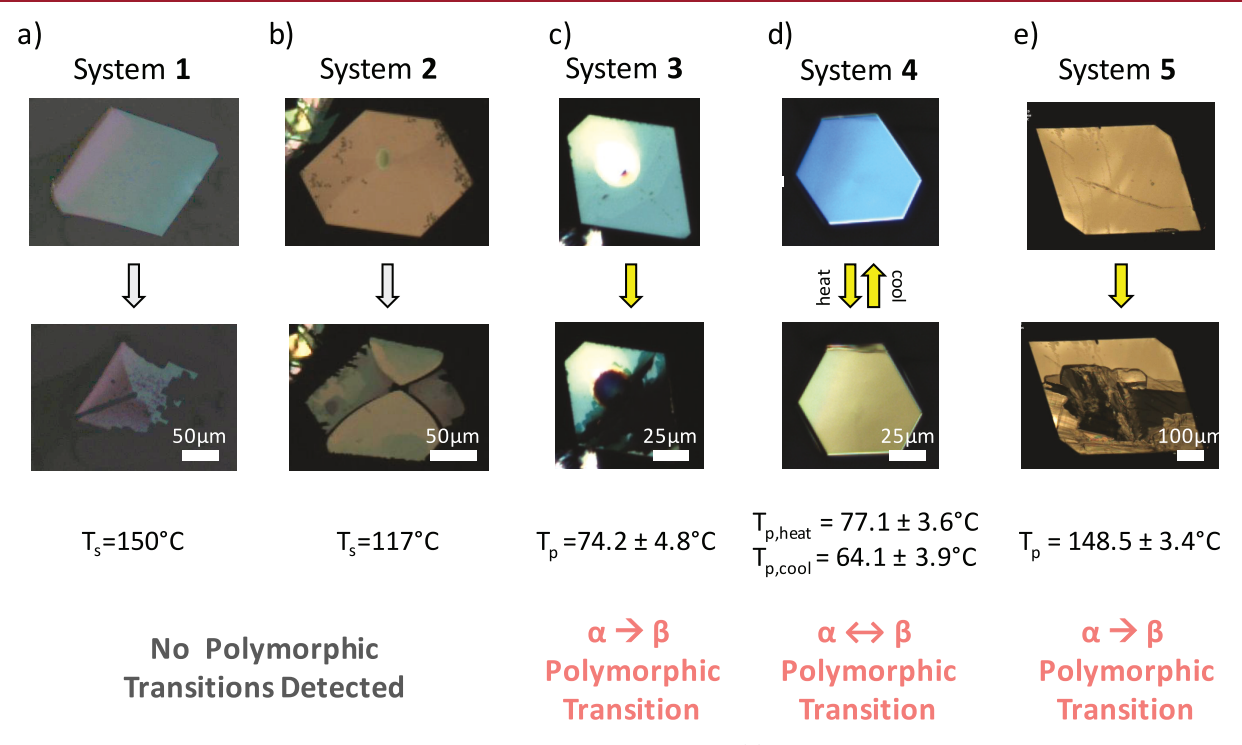


Figure 2. CPOM to observe polymorph transition in single crystals of BTBT systems. (a) System 1 shows no polymorphic transition, in agreement with the DSC result. The sublimation point  $(T_s)$  is at 150 °C. (b) System 2 shows no polymorphic transition, in agreement with the DSC result. The sublimation point  $(T_s)$  is at 117 °C. (c) System 3 shows a clear polymorphic transition from  $\alpha$  to  $\beta$  upon heating. The transition point  $(T_p)$  was averaged over 15 single crystals. (d) System 4 shows a clear reversible polymorphic transition from  $\alpha$  to  $\beta$  upon heating and cooling. The transition points  $(T_p s)$  were averaged over 35 single crystals. (e) System 5 shows a clear polymorphic transition from  $\alpha$  to  $\beta$  upon heating. The transition point  $(T_p)$  was averaged over 10 single crystals.

## RESULTS

Polymorphic Phase Space of BTBT Systems. Five organic semiconductor systems with a common BTBT core were synthesized according to previous work.<sup>22–24</sup> System 1 contains no side chains, and system 2 has a single *tert*-butyl (tBu) side chain from the BTBT core. Systems 3–5 contain isopropyl (diiPr), *tert*-butyl (ditBu), and trimethylsilyl (diTMS) side chains on both ends, respectively, of increasing bulkiness. System 4 is bulkier than 3, as it contains an

additional methyl group, and system 5 is bulkier than 4, as substituting the central carbon with the silicon atom increases the bond length by 22% (carbon–carbon 1.54 Å, silicon–carbon 1.88 Å, measured from Mercury v.3.9<sup>25</sup>).

First, we investigate the polymorphic phase space of these systems by differential scanning calorimetry (DSC), shown in Figure 1. Interestingly, while 1 and 2 do not show any peaks before melting, 3–5 show endothermic peaks upon heating at 69.6, 71.0, and 150.9 °C, respectively. This occurs well below

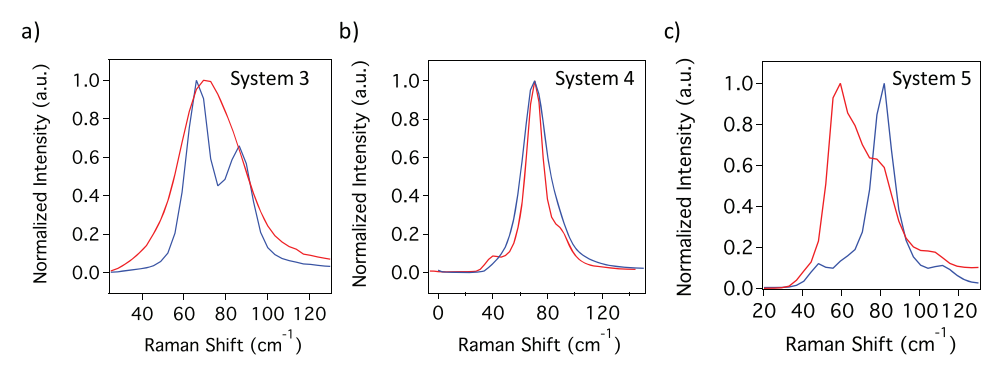


Figure 3. Phonon region of the Raman spectra to identify polymorphs in systems 3–5. All spectra were normalized. Blue spectra indicate the  $\alpha$  polymorph, and red spectra indicate the  $\beta$  polymorph for each system. For all three systems, each polymorph was clearly identifiable from the phonon regions.

their melting points, <sup>22,26</sup> 195.6, 277.1, and 215.3 °C, respectively, indicating a possible crystal—crystal transition. Systems 4 and 5 show reversible exothermic peaks upon cooling at temperatures 69.0 and 146.8 °C. The heat of transition rule<sup>27</sup> indicates an enantiotropic<sup>28</sup> relationship between polymorphs when an endothermic phase change is observed upon heating. Since 3–5 all displayed an endothermic phase change upon heating, we believe 3 should also be enantiotropic and the DSC results should actually be similar to those 4 and 5. Thus, we suspect 3 to be a case of kinetically irreversible enantiotropic polymorphs, <sup>29,30</sup> where the transformed polymorph of 3 was kinetically restrained from reversing back to the powder form. This kinetic irreversibility is observed again in single crystals of both 3 and 5, which we will discuss later.

We formed single crystals of the systems for direct observation of polymorphic transition behavior using a cross-polarized optical microscope (CPOM) equipped with a heating stage. Single crystals are an excellent platform to visualize polymorphic transitions. In fact, phenomenological differences in their transitions from CPOM can even lead to distinction in their polymorphic transition mechanisms, as discussed in our previous work. Single crystals were formed by drop-casting a slightly supersaturated solution onto clean silicon substrates. A variety of solvents were used to screen for polymorphs during single-crystal formation. Specific experimental conditions are given in Materials and Methods and Table S1. Polymorph identification of the as-formed single crystals was carried out using single-crystal X-ray diffraction (SCXRD) and Raman spectroscopy.

Under CPOM with a Linkam heatstage, the crystals were heated and cooled at a rate of 10 °C min<sup>-1</sup>. Consistent with the DSC results, 1 and 2 showed no transition behavior before sublimation, while 3-5 showed polymorphic phase transitions (Figure 2and Movies S1-S5). We defined a polymorphic transition when the single-crystal sample showed a clear distinct change in the birefringence under CPOM. A distinct change in the birefringence indicates change in the refractive index ellipsoid, which results from a structural change. Clear birefringence changes occur for system 3-5, while systems 1 and 2 only showed sublimation. Sublimation points are displayed for 1 and 2, and average transition points are shown for 3-5 obtained from 15, 35, and 10 crystals, respectively. We note that because the single crystals are very thin (ca. hundreds of micrometers in thickness), they sublime before melting. These values are calibrated by directly measuring the substrate temperature. The calibrated values

differ from the Linkam heating stage temperatures displayed in Movies S1–S5. For convenience, we denote the polymorph stable at room temperature as the  $\alpha$  form and the higher temperature form as the  $\beta$  form for 3–5. To identify the  $\alpha$  and  $\beta$  polymorphs of 3–5, we utilized the low-frequency region of Raman spectroscopy associated with crystal lattice vibrations. Low-frequency Raman spectroscopy is often utilized in the pharmaceutical industry to identify polymorphs, <sup>32,33</sup> as shown in Raman spectra of the polymorphs in Figure 3.

Interestingly, in single crystals, only 4 showed reversibility, while both 3 and 5 were irreversible after the heating transition. In system 3, the irreversibility is consistent with the DSC results, indicating that both the powder and single crystals of 3 could not overcome the kinetic energy barrier to transition back. However, in 5, the irreversibility was only observed on single crystals, as DSC showed a reversible transition. To match the polymorph of the powders to the single crystals used in CPOM experiments, we conducted powder X-ray diffraction (pXRD) on all five systems (Figure S1). Surprisingly, when powder X-ray diffraction was used on the powder samples of 3 and 5 used for DSC (Figure S2), powders of system 3 contained both  $\alpha$  and  $\beta$  forms and powders of system 5 showed an additional peak at lower  $2\theta$ indicating a third polymorph in addition to the  $\alpha$  and  $\beta$  forms. The third polymorph may be linked to the reversibility of polymorph transitions in powder samples of 5. However, we were not able to validate this point, as the third polymorph was not accessible in single-crystal forms despite solvent screening. In fact, through the solvent screening process, only two polymorphs were discovered each for 3-5.

Polymorph Structure Characterizations Using **SCXRD.** Essential to investigating the molecular origin of polymorphism is SCXRD, which is a powerful tool to observe the molecular packing. From the specific structural modifications, we can investigate the role of added side chains in the changes in structure. We acquired the structural information on all five systems and their polymorphs from single crystals formed from drop-casting (Table S1) and from previous works.<sup>22,24</sup> We note that, in our previous work,<sup>22</sup> the reported structures for 3-5 correspond to the  $3\beta$ ,  $4\alpha$ , and  $5\alpha$ forms in this study. Despite changes in the molecule, all five systems showed a herringbone packing motif, with the layers stacking along the a axis of the unit cell, as displayed from Bravais-Friedel-Donnay-Harker (BFDH) morphology calculations (Figure S3). Interestingly, for the five systems studied here, the slight molecular structural changes were not sufficient to alter the packing motif, in contrast to systems in other

Table 1. Crystallographic Data of All BTBT Systems and Their Polymorphs

	1	2	$3\alpha$	$3\beta$	$4\alpha$	$4\beta$	$5\alpha$	5β
T (K)	123	90	100	90	123	370	100	100
space group	$P2_1/c$	$P2_{1}2_{1}2_{1}$	$P2_1/c$	$P2_1/c$	$P2_1/c$	$P2_1/c$	$P\overline{1}$	$P2_1/c$
a (Å)	5.85	6.06	6.13	6.24	6.04	6.33	7.43	6.30
b (Å)	7.96	7.70	8.21	11.75	10.55	10.42	10.04	11.14
c (Å)	11.81	30.80	16.04	11.50	14.02	14.63	13.53	14.28
$\alpha$ (deg)	74	90	82.59	85	88.46	86.25	82.83	88.53
$\beta$ (deg)	90	90	90	90	90	90	82.08	90
γ (deg)	90	90	90	90	90	90	88.63	90
V (Å <sup>3</sup> )	528.98	1437.80	800.46	840.05	893.99	962.47	992.19	1001.8

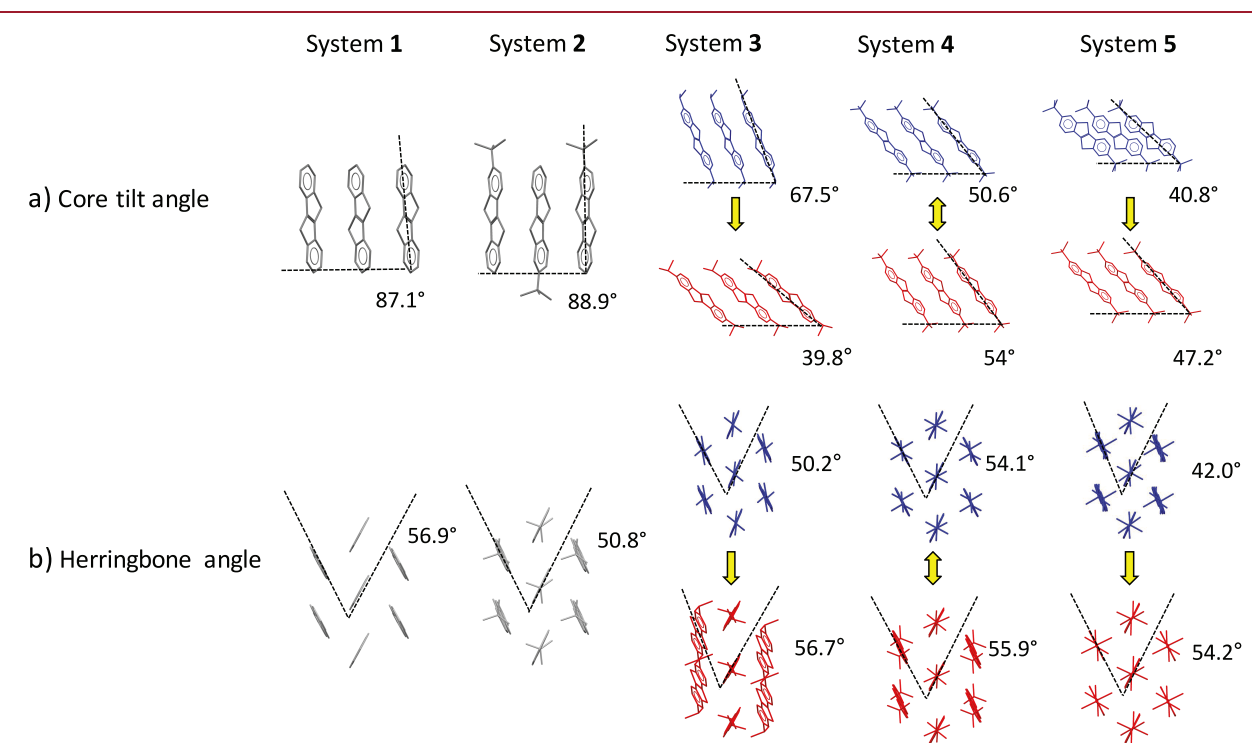
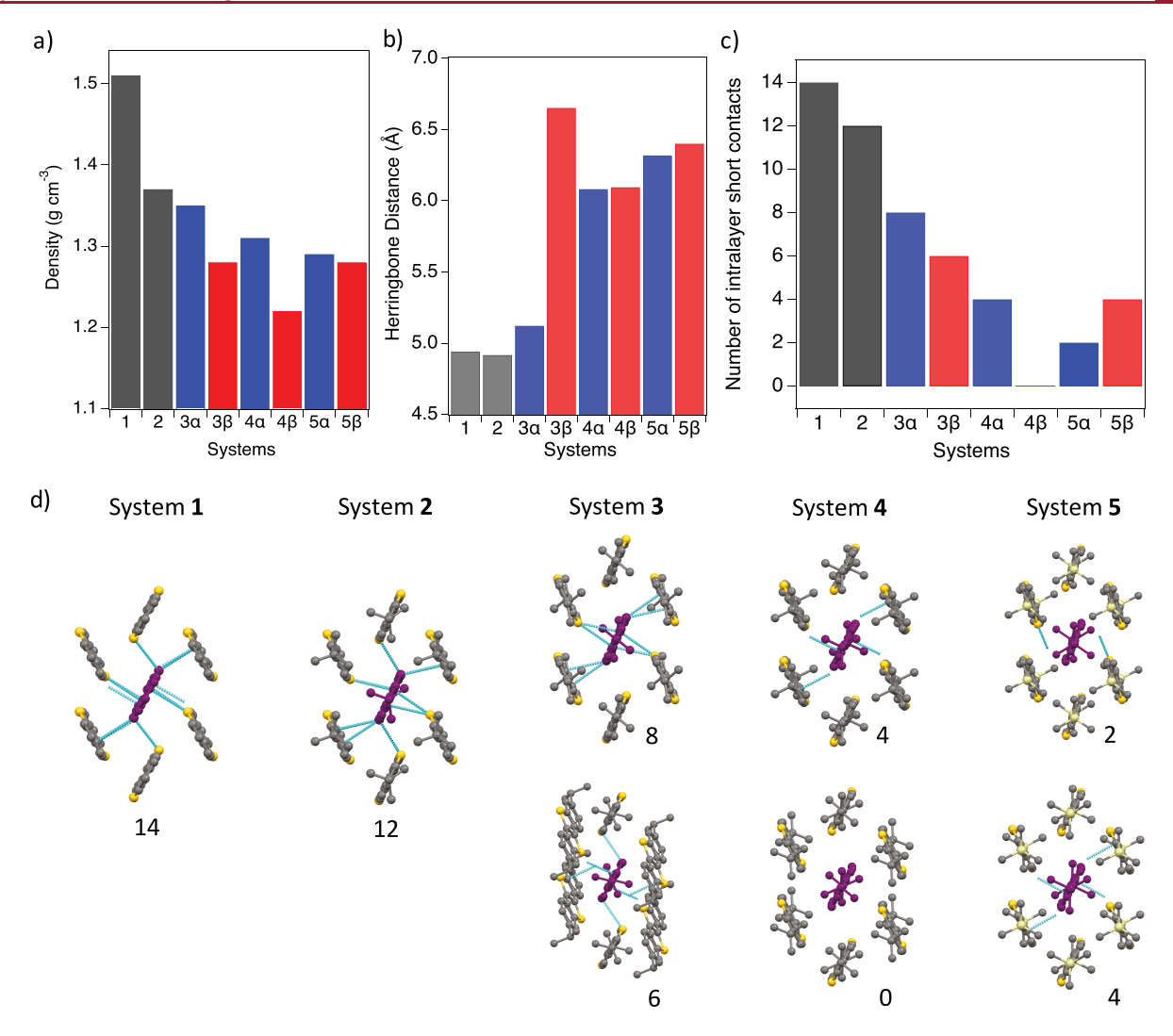


Figure 4. Molecular packing of BTBT systems. For systems 3–5, blue structures indicate the  $\alpha$  form and red structures indicate the  $\beta$  form. In all structures, the (a) core tilt angle and (b) herringbone angle are measured within a single layer of molecules. For the herringbone configuration, the viewing axis is along the long axis of the center molecule. Consequently, as shown in system  $3\beta$ , the neighboring molecules from the center molecule are significantly tilted away from their long axis.

works<sup>34,35</sup> that experienced a change in the packing motif after a slight change in the structure. Unit cell parameters of all systems and their polymorphs are given in Table 1. We point out that, for  $4\alpha$  and  $4\beta$ , the structural changes are very small, since the polymorphic transition involves a cooperative, or displacive, transition mechanism, as shown in our previous work.<sup>36</sup> One may attribute such small structural change to thermal expansion, but as discussed extensively in our previous works,<sup>8,37</sup> a drastic optical, electronic, first-order polymorph transition indeed occurs in system 4.

Across the five systems, we first compare two major characteristics of the molecular packing, the core tilt angle and the herringbone angle, in Figure 4. All structures were collected at low temperatures (90–123 K), with the exception of  $4\beta$ , which was only accessible at a high temperature of 370 K. We note that whole-molecule disorder was present in systems 2 and  $3\beta$  and rotational disorder was present in side chains of  $4\beta$ , as shown in Figure S4. All disordered portions were disregarded for angle measurements.

Interestingly, from system 1 to 5, the core tilt angle shows a drastic change when the stable forms are compared (bluecolored  $\alpha$  forms for 3-5). The largest difference is seen on comparing 1 and 2, which have either no side chain or only a single side chain, with 3-5, which have side chains on both ends of the BTBT core. Both 1 and 2 have very similar tilt angles of almost 90°, indicating that the core stays almost upright. Molecules in 2 stack in an antiparallel fashion, with the side chain packing on opposite sides of the core in a herringbone pair; in a  $\pi$ - $\pi$  pair the side chains are on the same side. Such a packing arrangement implies that the sidechain interactions may be very weak, if at all, given the longer  $\pi$ - $\pi$  distance (6.065 Å) in comparison to the herringbone distance (4.916 Å) (Figure S5). Thus, it is not surprising that 2 can pack similarly to 1, which does not have any side chains. However, as side chains are added to both ends, the molecules become more tilted in the crystal lattice. From 3 to 5, as the bulkiness of the side chains increases, the core tilt angle decreases, from 67.5 to 50.6 and 40.8°. The core tilt angles of 3-5 after transition (displayed in red in Figure 4) are also



Number of short contacts from center molecule

Figure 5. Effect of side chain design on packing density and intralayer short contacts. (a) Calculated density of all systems from single-crystal structures showing a decreasing trend from 1 to 5. For systems 3–5, blue bars indicate  $\alpha$  forms and red bars indicate  $\beta$  forms. (b) Measured herringbone distance in systems 1–5 for the stable  $\alpha$  form at ambient conditions. (c) Number of intralayer short contacts experienced by a reference molecule in a herringbone configuration for all systems. For systems 3–5, blue bars indicate  $\alpha$  forms and red bars indicate  $\beta$  forms. (d) Schematic of the intralayer short contacts, depicted by cyan dashed lines, experienced by the center reference molecule, depicted in purple.

much lower than those of 1 and 2. Specifically for 3, the change in angle is significant, from 67.5 to 39.8°, which may explain the irreversibility of the polymorph transition in powder and single-crystal forms due to a possible high transition barrier.

For the herringbone angles, however, there was no trend as the side chains were added. The angle change for 5 polymorphs was significant from 42 to 54.2°, while 3 and 4 polymorphs showed smaller changes. We note that 4 polymorphs showed the least core tilt and herringbone angle changes, and this is directly related to the polymorphic transition mechanism, which is a cooperative transition.<sup>31</sup> In contrast, the large core tilt angle change in 3 and herringbone angle change in 5 underlie their nucleation and growth<sup>30,38</sup> polymorph transition mechanism.

Moreover, we measured the pitch and roll angles and distances of the five systems and their polymorphs, as analyzed by Curtis and colleagues.<sup>39</sup> The results are included in Table S2. Similar to herringbone angles, no clear trend was detected

as the side chain bulkiness increased. However, between the  $\alpha$  and  $\beta$  polymorphs in systems 3 and 5, large changes in the pitch angle and distances were observed, indicating that structural changes between polymorphs can be significant.

Overall, we show that the addition of side chains in our systems did not change the packing motif of the crystals. The most notable effect of side chains is in the core tilt angle, as 3–5 experience lower angles than 1 and 2, which are close to 90°. Also in 3–5 we observe a systematic decrease in the core tilt angle as the bulkiness of the side chains increases. However, the addition of bulky side chains did not have an obvious effect on the herringbone angle or the pitch and roll angles and distances of the crystal packing.

Next, we look at the packing density and the intermolecular distance between neighboring molecules to investigate the role of side chains. Figure 5a and Table S3 show the calculated density in each system obtained from crystal structures, as well as the percent change from 1, which has the highest density. There is a clear decreasing trend in density, with 1 being

significantly higher than all other systems. The decrease in density from 1 to 2 was ca. 9.3%, while the decrease in density from 1 to  $3\alpha$  was ca. 10.6% (Table S3). This small change between 2 and  $3\alpha$  shows that even a single tBu arm attached to the core loosens the packing environment in comparison to having diiPr side chains attach on both ends. However, when the density of 2 is compared to that of  $4\alpha$ , which has the same tBu group on both ends instead of on one end of the core, the packing is much tighter in 2, as the density dropped from 1.37 to 1.31 g cm<sup>-1</sup> when one more tBu group was added. With an increase in bulkiness of the side chains from 3 to 5, the density of the  $\alpha$  form consistently decreases, indicating that bulkier side chains loosen the molecular packing. For polymorphs of the same compound, we consistently observed a decrease in density from  $\alpha$  to  $\beta$  polymorphs for 3-5. In fact, the  $\beta$ polymorphs always showed a lower density in comparison the  $\alpha$  form in each system, in agreement with the density rule<sup>2</sup> which indicates that the stable structure at lower temperature has the more efficient packing and hence the higher density.

Looser packing as bulkier side chains are added to the core indicate that the physical distance between the molecules will also increase. Quantifiable parameters are the closest intermolecular distances, which correspond to the distance in the herringbone pair (Figure 5b and Table S3). This distance was measured in Mercury v3.9. between the centers of the BTBT cores from the SCXRD structures. For systems 2 and  $5\alpha$  where two different herringbone distances exist, the greater distance was used in Figure 5b. In the case of herringbone distances, the role of having side chains on both ends is pronounced, as there is a larger increase in the distance in systems 3-5 in comparison to systems 1 and 2. The increase in system 1 from 2 is only ca. 0.5%, while the increases in systems 3-5 from 2 are much larger at ca. 4.2%, 23.7%, and 28.5%, respectively. Systems 4 and 5 also have a significantly higher herringbone distance in comparison to 3, as these have much bulkier tBu and TMS side chains in comparison to the

Other parameters that depict how close the molecules are the short contacts. Short contacts exist in neighboring molecules if the measured distance between two neighboring atoms is smaller than the sum of the van der Waals radii of the atoms. 40 We observe that comparing the number of short contacts with a reference molecule in each crystal structure indicates the relative tightness of the packing. The more short contacts that a reference molecule experiences, the more dense the packing can be. We point out that the short contacts defined here are adopted directly from Mercury v.3.9, in which all interactions including hydrogen-hydrogen interactions are considered. The number of short contacts between a reference molecule with its six nearest neighbors in  $\pi$ – $\pi$  and herringbone pairs was considered in all systems (Figure 5c,d and Table S4). The reference molecules in systems 1 and 2 experience 14 and 12 short contacts from all 6 of their surrounding molecules, while the number systematically decreases with added side chains. The reference molecules in all polymorphs of systems 3-5 have a lower number of short contacts only from four or fewer neighboring molecules. This observation supports the hypothesis that the side chains on both ends create space in the packing, allowing more room for the molecules. Because the molecules are less interlocked in systems 3-5, they can adopt multiple packings, leading to the polymorphism observed.

The calculated density, herringbone distance, and number of short contacts all indicate the role of side chains in decreasing the packing density. The bulky side chains loosen the packing in the crystal lattice, allowing an environment favorable for multiple packing states accessible by inputting thermal energy. Thus, adding bulky side chains in molecular systems could serve as a molecular design rule to trigger polymorphism in organic electronic systems.

In summary, we investigated the effect of side chains on polymorphism by a systematic study of five organic semiconductors containing the BTBT core with varying side chain environments. We explored the polymorphic phase space in the bulk and single crystals and discovered polymorphs only in systems with side chains on both ends of the core. We accessed the crystal structures via SCXRD and observed various changes to the packing structure, such as a systematic decrease in the core tilt angle as bulkier side chains are added on. However, even with different side chains, all five systems had the same herringbone packing motif. We analyzed key parameters that provide information on changes in the packing environment such as calculated density, intermolecular distance, and number of short contacts. The decrease in density, increase in intermolecular distance, and decrease in the number of short contacts from bare BTBT to diTMS-BTBT indicated that the added bulky side chains produce motifs that are less densely packed in the crystal structure. Moreover, as the side chains get bulkier from diiPr to ditBu to diTMS, the effect is stronger.

This hypothesis of increased side-chain bulkiness leading to a decrease in packing density was confirmed in two other studies, in a study of bulky side chains on oligothiophenes by Kreyes and colleagues<sup>41</sup> and in a study of increase in bulkiness of side chains in pentacene derivatives by Pensack and colleagues.<sup>42</sup> We note that this trend is specific to branched bulky side chain substituents, as Inoue and colleagues<sup>43</sup> have shown that, for linear alkyl chains, longer chains can densify and increase the cohesive energy, demonstrating a "zipper effect". Moreover, one primary example of an organic semiconductor with added bulky side chains is TIPSpentacene, which has been reported<sup>7,8</sup> to show numerous polymorphs, again confirming our hypothesis. Our results suggest that, for this organic electronic materials class, the addition of bulky side-chain substituents to the conjugated core serves to introduce polymorphs in the crystal structures.

## MATERIALS AND METHODS

Materials Synthesis. Details of the synthesis steps for system 1 ([1]benzothieno[3,2-b]benzothiophene (BTBT)), 2 (tert-butyl BTBT), 3 (disopropyl BTBT), 4 (di-tert-butyl BTBT), and 5 (bis(trimethylsilyl) BTBT) have been given in previous work. 22,24

**Single-Crystal Sample Preparation.** Details of forming single crystals of ditBu are included in previous work. For diiPr samples used for in situ microscopy, a stock solution of decane, tetralin, or dimethylformamide (DMF) was used to obtain the  $\alpha$  polymorph. The  $\beta$  polymorph was not obtainable from drop-casting and only was accessed from sublimation in our previous work. The stock solutions used had a concentration of approximately 10 mg mL<sup>-1</sup> for all three solvents. A 5-10 μL amount of the solution was dropcasted onto silicon substrates. Larger single crystals for single-crystal X-ray diffraction (SCXRD) were formed from 10–20 μL of solution drop-casted onto indented glass wellplates (Pyrex spot plates). For diTMS samples used for in situ microscopy, a stock solution of tetralin in concentrations ranging from 6 to 11 mg mL<sup>-1</sup> were mainly used for drop-casting. Up to 2–5 μL of the solution was drop-casted directly onto silicon substrates or onto nine-well glass plates for slow evaporation overnight.  $\alpha$  crystals usually formed with

solutions at higher concentration ( $\sim$ 10 mg mL $^{-1}$ ) and  $\beta$  crystals at lower concentration ( $\sim$ 6 mg mL $^{-1}$ ). To form larger single crystals of diTMS for SCXRD,  $\alpha$  crystals could only be obtained by seed crystallization of a previously drop-casted  $\alpha$  crystal in ethyl acetate (2 mg mL $^{-1}$ ) for slow evaporation.  $\beta$  crystals were obtained from slow evaporation in toluene (5 mg mL $^{-1}$ ), acetone (1 mg mL $^{-1}$ ), or chloroform (5 mg mL $^{-1}$ ). Table S1 summarizes all conditions for forming single crystals of all systems. The Cambridge Crystallographic Data Center numbers for all structures, including ones from previous works, <sup>22,24</sup> are 1 (1025732), 2 (1008118), 3 $\alpha$  (1959510), 3 $\beta$  (1008120), 4 $\alpha$  (1008575), 4 $\beta$  (1570909), 5 $\alpha$  (1008576), and 5 $\beta$  (1959511).

Cross-Polarized Optical Microscopy (CPOM). Single crystals on silicon substrates were placed in a heating chamber with Linksys32 temperature control under a Nikon H550S instrument with a high-speed camera (Infinity 1). The heating chamber was capped with a sealable lid during heating and cooling cycles, and the rate was kept constant at 10 °C min<sup>-1</sup>. Time-lapse images were taken for all in situ experiments with various frame rates ranging from 1 to 10 fps. Image analysis was performed with softwares Nikon NIS Elements, Linksys32 data capture, and ImageJ.

**Single-Crystal X-ray Diffraction.** The single-crystal structures for the ditBu  $\beta$  form at 370 K and the diTMS  $\beta$  form at 100 K were collected at the G. L. Clark X-ray facility at the University of Illinois at Urbana—Champaign. Diffraction data were collected on a Bruker D8 Venture instrument equipped with a four-circle kappa diffractometer and Photon 100 detector. An I $\mu$ s microfocus Mo ( $\lambda$  = 0.71073 Å) source supplied the multimirror monochromated incident beam. The sample was mounted on a 0.3 mm loop with a minimal amount of Paratone-N oil. Data were collected as a series of  $\varphi$  and  $\omega$  scans at the corresponding temperatures for the two systems. Data were integrated and filtered for statistical outliers using SAINT (Bruker, 2014) and then corrected for absorption by integration using SADABS v2014/4 (Bruker, 2014). The structure was phased by direct methods and refined using the software package SHELX-2014-3 (Sheldrick, 2008).

The single-crystal structure for the diiPr  $\alpha$  form at 100 K was collected at NSF's ChemMatCARS (Sector 15) of the Advanced Photon Source, Argonne National Laboratory. The clear hexagonal plate crystals were mounted on a 5  $\mu$ m diameter glass fiber tip with epoxy. The beam energy was 30 keV (0.41328 Å), and the beam size at the sample was 0.15 × 0.15 mm<sup>2</sup>. Data were collected using a Huber three-circle diffractometer with a  $\kappa$  angle offset of 60° that was equipped with a Pilatus3X 1M(CdTe) detector. The distance between the detector and the crystal was 130 mm. A total of 720 frames were collected at two  $\theta$  angles sitting at  $0^{\circ}$  and  $\omega$  angles sitting at  $-180^{\circ}$ , followed up by two different  $\kappa = 0^{\circ}$  and  $\kappa = 15^{\circ}$ , respectively. The data were collected with the  $\phi$  angle scanned over a range of 360° using a shutterless mode. User-friendly data collection software was used. Tiff frames were converted to Bruker sfrm format. Data integration were performed with APEX II suite software. The reduction of data was conducted with SAINT v.8.32B and SADABS v.2013 programs included in the APEX suite. The structure solution and refinement were carried out with SHELX software using the XPREP utility for the space group determination and the XT and XL programs for the structure solution and refinement, respectively.

Raman Spectroscopy. Raman spectra were taken from single crystals grown on Si substrates, identical with the samples made for in situ microscopy experiments. A Raman confocal imaging microscope with a 532 nm laser (Laser Quantum Ventus 532 with maximum power 50 mW) and 50× long working distance objective lens (Horiba LabRAM HR 3D) equipped with a Horiba Synapse back-illuminated deep-depletion CCD camera was used to collect spectra. Using a 300 g mm<sup>-1</sup> grating, a scan exposure time of 10 s was used. An optical density filter of OD = 0.3 was used (OD = log(power transmission factor)), and no beam damage on the sample was observed. For variable-temperature experiments, the samples were collected using a Linkam THMS600 heating stage with a closed chamber. The heating and cooling rates were kept at 10 °C min<sup>-1</sup>.

X-ray Diffraction. Powder samples of diiPr and diTMS-BTBT were used to collect powder XRD data. They were collected on a

Rigaku MiniFlex 600 diffractometer (SN BD63000258-03). Measurements employed Ni-filtered Cu K $\alpha$  ( $\lambda$  = 1.54178 Å) radiation from a copper sealed tube with 40 kV voltage and 15 mA current in the Bragg–Brentano geometry. Diffraction patterns were measured over the range of 3–100°  $2\theta$  by step scanning at a rate of 1 s/0.02°.

# ASSOCIATED CONTENT

# **Supporting Information**

he Supporting Information is available free of charge on the ACS publications Web site at The Supporting Information is available free of charge at https://pubs.acs.org/doi/10.1021/acs.cgd.9b01372.

Movies showing systems 1–5 under CPOM upon heating (ZIP)

Figures and tables as described in the text and descriptions of movies (PDF)

## **Accession Codes**

CCDC 1959510-1959511 contain the supplementary crystallographic data for this paper. These data can be obtained free of charge via <a href="www.ccdc.cam.ac.uk/data\_request/cif">www.ccdc.cam.ac.uk/data\_request/cif</a>, or by emailing <a href="mailto:data\_request@ccdc.cam.ac.uk">data\_request@ccdc.cam.ac.uk</a>, or by contacting The Cambridge Crystallographic Data Centre, 12 Union Road, Cambridge CB2 1EZ, UK; fax: +44 1223 336033.

# AUTHOR INFORMATION

## **Corresponding Author**

Ying Diao — Department of Chemical and Biomolecular Engineering, University of Illinois at Urbana—Champaign, Urbana, Illinois 61801, United States; orcid.org/0000-0002-8984-0051; Email: yingdiao@illinois.edu

## **Authors**

Hyunjoong Chung – Department of Chemical and Biomolecular Engineering, University of Illinois at Urbana–Champaign, Urbana, Illinois 61801, United States

Shanwen Chen – Department of Chemical and Biomolecular Engineering, University of Illinois at Urbana–Champaign, Urbana, Illinois 61801, United States

Bijal Patel — Department of Chemical and Biomolecular Engineering, University of Illinois at Urbana—Champaign, Urbana, Illinois 61801, United States

Guillaume Garbay – Laboratoire de Chimie des Polymères Faculté des Sciences, Université Libre de Bruxelles (ULB), 1050 Brussels, Belgium

Yves H. Geerts — Laboratoire de Chimie des Polymères Faculté des Sciences, Université Libre de Bruxelles (ULB), 1050 Brussels, Belgium; orcid.org/0000-0002-2660-5767

Complete contact information is available at: https://pubs.acs.org/10.1021/acs.cgd.9b01372

#### **Notes**

The authors declare no competing financial interest.

## ACKNOWLEDGMENTS

Y.D. acknowledges the Sloan Foundation for the Sloan Research Fellowship in Chemistry and 3M Nontenured Faculty Award that supported this work. H.C. acknowledges the Glenn E. and Barbara R. Ullyot Graduate Fellowship and the A. T. Widiger Fellowship. This work was conducted in part in the Frederick Seitz Materials Research Laboratory Central Facilities, G. L. Clark X-ray facility and the Beckman Institute for Advanced Science and Technology at the University of

Illinois at Urbana-Champaign. Single-crystal structures were obtained at the ChemMatCARS Sector, supported by the National Science Foundation under grant number NSF/CHE-1834750. Portions of this research were carried out at the Advanced Photon Source, a U.S. Department of Energy (DOE), Office of Science User Facility, operated for the DOE Office of Science by Argonne National Laboratory under Contract No. DE-AC02-06CH11357. We thank Dr. Jeffrey Alan Bertke for collecting and solving polymorphs of ditBu single crystals and Dr. Toby J. Woods for collecting and solving polymorphs of diTMS single crystals. We thank Dr. SuYin Grass Wang, Dr. YuSheng Chen, and Tieyan Chang for help in setting up the single crystal X-ray diffraction experiments at Argonne National Laboratory. Y.H.G. is thankful to the Belgian National Fund for Scientific Research (FNRS) for financial support through research projects BTBT no. 2.4565.11, Phasetrans no. T.0058.14, Pi-Fast no. T.0072.18, and 2Dto3D no. 30489208. Financial support from the French Community of Belgium (ARC no. 20061) and from the Walloon Region (WCS no. 1117306, SOLIDYE no. 1510602) is also acknowledged.

# REFERENCES

- (1) Stevens, L. A.; Goetz, K. P.; Fonari, A.; Shu, Y.; Williamson, R. M.; Brédas, J. L.; Coropceanu, V.; Jurchescu, O. D.; Collis, G. E. Temperature-Mediated Polymorphism in Molecular Crystals: The Impact on Crystal Packing and Charge Transport. *Chem. Mater.* **2015**, 27, 112–118.
- (2) Brédas, J. L.; Calbert, J. P.; da Silva Filho, D. A.; Cornil, J. Organic semiconductors: A theoretical characterization of the basic parameters governing charge transport. *Proc. Natl. Acad. Sci. U. S. A.* **2002**, *99*, 5804–5809.
- (3) Sutton, C.; Risko, C.; Bredas, J. L. Noncovalent Intermolecular Interactions in Organic Electronic Materials: Implications for the Molecular Packing vs Electronic Properties of Acenes. *Chem. Mater.* **2016**, 28, 3–16.
- (4) Mas-Torrent, M.; Rovira, C. Role of Molecular Order and Solid-State Structure in Organic Field-Effect Transistors. *Chem. Rev.* **2011**, 111, 4833–4856.
- (5) Chung, H.; Diao, Y. Polymorphism as an emerging design strategy for high performance organic electronics. *J. Mater. Chem. C* **2016**, *4*, 3915–3933.
- (6) Chen, J.; Anthony, J.; Martin, D. C. Thermally Induced Solid-State Phase Transition of Bis(triisopropylsilylethynyl) Pentacene Crystals. *J. Phys. Chem. B* **2006**, *110*, 16397–16403.
- (7) Diao, Y.; Lenn, K. M.; Lee, W.-Y.; Blood-Forsythe, M. A.; Xu, J.; Mao, Y.; Kim, Y.; Reinspach, J. A.; Park, S.; Aspuru-Guzik, A.; Xue, G.; Clancy, P.; Bao, Z.; Mannsfeld, S. C. B. Understanding Polymorphism in Organic Semiconductor Thin Films through Nanoconfinement. J. Am. Chem. Soc. 2014, 136, 17046—17057.
- (8) Chung, H.; Dudenko, D.; Zhang, F. J.; D'Avino, G.; Ruzie, C.; Richard, A.; Schweicher, G.; Cornil, J.; Beljonne, D.; Geerts, Y.; Diao, Y. Rotator side chains trigger cooperative transition for shape and function memory effect in organic semiconductors. *Nat. Commun.* **2018**, *9*, 278.
- (9) Jurchescu, O. D.; Mourey, D. A.; Subramanian, S.; Parkin, S. R.; Vogel, B. M.; Anthony, J. E.; Jackson, T. N.; Gundlach, D. J. Effects of polymorphism on charge transport in organic semiconductors. *Phys. Rev. B: Condens. Matter Mater. Phys.* **2009**, *80*, 085201.
- (10) Chen, J.; Shao, M.; Xiao, K.; Rondinone, A. J.; Loo, Y.-L.; Kent, P. R. C.; Sumpter, B. G.; Li, D.; Keum, J. K.; Diemer, P. J.; Anthony, J. E.; Jurchescu, O. D.; Huang, J. Solvent-type-dependent polymorphism and charge transport in a long fused-ring organic semiconductor. *Nanoscale* **2014**, *6*, 449–456.
- (11) Käfer, D.; Ruppel, L.; Witte, G.; Wöll, C. Role of Molecular Conformations in Rubrene Thin Film Growth. *Phys. Rev. Lett.* **2005**, 95, 166602.

- (12) Matsukawa, T.; Yoshimura, M.; Uchiyama, M.; Yamagishi, M.; Nakao, A.; Takahashi, Y.; Takeya, J.; Kitaoka, Y.; Mori, Y.; Sasaki, T. Polymorphs of Rubrene Crystal Grown from Solution. *Jpn. J. Appl. Phys.* **2010**, *49*, 085502.
- (13) He, T.; Stolte, M.; Burschka, C.; Hansen, N. H.; Musiol, T.; Kalblein, D.; Pflaum, J.; Tao, X. T.; Brill, J.; Wurthner, F. Single-crystal field-effect transistors of new Cl-2-NDI polymorph processed by sublimation in air. *Nat. Commun.* **2015**, *6*, 5954.
- (14) Pfattner, R.; Mas-Torrent, M.; Bilotti, I.; Brillante, A.; Milita, S.; Liscio, F.; Biscarini, F.; Marszalek, T.; Ulanski, J.; Nosal, A.; Gazicki-Lipman, M.; Leufgen, M.; Schmidt, G.; Molenkamp, L. W.; Laukhin, V.; Veciana, J.; Rovira, C. High-Performance Single Crystal Organic Field-Effect Transistors Based on Two Dithiophene-Tetrathiafulvalene (DT-TTF) Polymorphs. Adv. Mater. 2010, 22, 4198–4203.
- (15) Gentili, D.; Gazzano, M.; Melucci, M.; Jones, D.; Cavallini, M. Polymorphism as an additional functionality of materials for technological applications at surfaces and interfaces. *Chem. Soc. Rev.* **2019**, *48*, 2502–2517.
- (16) Hiszpanski, A. M.; Lee, S. S.; Wang, H.; Woll, A. R.; Nuckolls, C.; Loo, Y. L. Post-deposition Processing Methods To Induce Preferential Orientation in Contorted Hexabenzocoronene Thin Films. ACS Nano 2013, 7, 294–300.
- (17) Hiszpanski, A. M.; Baur, R. M.; Kim, B.; Tremblay, N. J.; Nuckolls, C.; Woll, A. R.; Loo, Y. L. Tuning Polymorphism and Orientation in Organic Semiconductor Thin Films via Post-deposition Processing. *J. Am. Chem. Soc.* **2014**, *136*, 15749–15756.
- (18) Purdum, G. E.; Yao, N.; Woll, A.; Gessner, T.; Weitz, R. T.; Loo, Y.-L. Understanding Polymorph Transformations in Core-Chlorinated Naphthalene Diimides and their Impact on Thin-Film Transistor Performance. *Adv. Funct. Mater.* **2016**, *26*, 2357.
- (19) Giri, G.; Verploegen, E.; Mannsfeld, S. C. B.; Atahan-Evrenk, S.; Kim, D. H.; Lee, S. Y.; Becerril, H. A.; Aspuru-Guzik, A.; Toney, M. F.; Bao, Z. Tuning charge transport in solution-sheared organic semiconductors using lattice strain. *Nature* **2011**, *480*, 504–508.
- (20) Diao, Y.; Tee, B. C. K.; Giri, G.; Xu, J.; Kim, D. H.; Becerril, H. A.; Stoltenberg, R. M.; Lee, T. H.; Xue, G.; Mannsfeld, S. C. B.; Bao, Z. Solution coating of large-area organic semiconductor thin films with aligned single-crystalline domains. *Nat. Mater.* **2013**, *12*, 665–671.
- (21) Riera-Galindo, S.; Tamayo, A.; Mas-Torrent, M. Role of Polymorphism and Thin-Film Morphology in Organic Semiconductors Processed by Solution Shearing. ACS Omega 2018, 3, 2329–2339.
- (22) Schweicher, G.; Lemaur, V.; Niebel, C.; Ruzie, C.; Diao, Y.; Goto, O.; Lee, W. Y.; Kim, Y.; Arlin, J. B.; Karpinska, J.; Kennedy, A. R.; Parkin, S. R.; Olivier, Y.; Mannsfeld, S. C. B.; Cornil, J.; Geerts, Y. H.; Bao, Z. N. Bulky End-Capped [1]Benzothieno[3,2-b]benzothiophenes: Reaching High-Mobility Organic Semiconductors by Fine Tuning of the Crystalline Solid-State Order. *Adv. Mater.* **2015**, *27*, 3066–3072.
- (23) Fernández, A. B.; Garcez da Veiga, A.; Aliev, A.; Ruzié, C.; Garbay, G.; Chattopadhyay, B.; Kennedy, A. R.; Geerts, Y. H.; Rocco, M. L. M. [1]Benzothieno[3,2-b]benzothiophene (BTBT) derivatives: Influence in the molecular orientation and charge delocalization dynamics. *Mater. Chem. Phys.* **2019**, 221, 295–300.
- (24) Niebel, C.; Kim, Y.; Ruzié, C.; Karpinska, J.; Chattopadhyay, B.; Schweicher, G.; Richard, A.; Lemaur, V.; Olivier, Y.; Cornil, J.; Kennedy, A. R.; Diao, Y.; Lee, W.-Y.; Mannsfeld, S.; Bao, Z.; Geerts, Y. H. Thienoacene dimers based on the thieno[3,2-b]thiophene moiety: synthesis, characterization and electronic properties. *J. Mater. Chem. C* 2015, 3, 674–685.
- (25) Macrae, C. F.; Bruno, I. J.; Chisholm, J. A.; Edgington, P. R.; McCabe, P.; Pidcock, E.; Rodriguez-Monge, L.; Taylor, R.; van de Streek, J.; Wood, P. A. Mercury CSD 2.0 new features for the visualization and investigation of crystal structures. *J. Appl. Crystallogr.* **2008**, *41*, 466–470.
- (26) Ebata, H.; Izawa, T.; Miyazaki, E.; Takimiya, K.; Ikeda, M.; Kuwabara, H.; Yui, T. Highly Soluble [1]Benzothieno[3,2-b]benzothiophene (BTBT) Derivatives for High-Performance, Solu-

- tion-Processed Organic Field-Effect Transistors. J. Am. Chem. Soc. 2007, 129, 15732–15733.
- (27) Burger, A.; Ramberger, R. On the polymorphism of pharmaceuticals and other molecular crystals. I. *Microchim. Acta* 1979, 72, 259–271.
- (28) Herbstein, F. H. On the mechanism of some first-order enantiotropic solid-state phase transitions: from Simon through Ubbelohde to Mnyukh. *Acta Crystallogr., Sect. B: Struct. Sci.* **2006**, 62, 341–383.
- (29) Kawakami, K. Reversibility of enantiotropically related polymorphic transformations from a practical viewpoint: Thermal analysis of kinetically reversible/irreversible polymorphic transformations. J. Pharm. Sci. 2007, 96, 982–989.
- (30) Krishnan, B. P.; Sureshan, K. M. A Spontaneous Single-Crystal-to-Single-Crystal Polymorphic Transition Involving Major Packing Changes. *J. Am. Chem. Soc.* **2015**, *137*, 1692–1696.
- (31) Chung, H.; Ruzie, C.; Geerts, Y.; Diao, Y. Hybrid Mechanism of Nucleation and Cooperative Propagation in a Single-Crystal-to-Single-Crystal Transition of a Molecular Crystal. *Cryst. Growth Des.* **2018**, *18*, 4245–4251.
- (32) Larkin, P. J.; Dabros, M.; Sarsfield, B.; Chan, E.; Carriere, J. T.; Smith, B. C. Polymorph Characterization of Active Pharmaceutical Ingredients (APIs) Using Low-Frequency Raman Spectroscopy. *Appl. Spectrosc.* **2014**, *68*, 758–776.
- (33) Brillante, A.; Bilotti, I.; Della Valle, R. G.; Venuti, E.; Masino, M.; Girlando, A. Characterization of phase purity in organic semiconductors by lattice-phonon confocal Raman mapping: Application to pentacene. *Adv. Mater.* **2005**, *17*, 2549–2553.
- (34) Dou, J.-H.; Zheng, Y.-Q.; Yao, Z.-F.; Yu, Z.-A.; Lei, T.; Shen, X.; Luo, X.-Y.; Sun, J.; Zhang, S.-D.; Ding, Y.-F.; Han, G.; Yi, Y.; Wang, J.-Y.; Pei, J. Fine-Tuning of Crystal Packing and Charge Transport Properties of BDOPV Derivatives through Fluorine Substitution. J. Am. Chem. Soc. 2015, 137, 15947–15956.
- (35) Sorli, J. C.; Ai, Q.; Granger, D. B.; Gu, K.; Parkin, S.; Jarolimek, K.; Telesz, N.; Anthony, J. E.; Risko, C.; Loo, Y.-L. Impact of Atomistic Substitution on Thin-Film Structure and Charge Transport in a Germanyl-ethynyl Functionalized Pentacene. *Chem. Mater.* **2019**, *31* (17), 6615–6623.
- (36) Dunitz, J. D. Phase-Transitions in Molecular-Crystals from a Chemical Viewpoint. *Pure Appl. Chem.* **1991**, *63*, 177–185.
- (37) Chung, H.; Chen, S.; Sengar, N.; Davies, D. W.; Garbay, G.; Geerts, Y. H.; Clancy, P.; Diao, Y. Single Atom Substitution Alters the Polymorphic Transition Mechanism in Organic Electronic Crystals. *Chem. Mater.* **2019**, *31*, 9115–9126.
- (38) Ito, H.; Muromoto, M.; Kurenuma, S.; Ishizaka, S.; Kitamura, N.; Sato, H.; Seki, T. Mechanical stimulation and solid seeding trigger single-crystal-to-single-crystal molecular domino transformations. *Nat. Commun.* **2013**, *4*, 2009.
- (39) Curtis, M. D.; Cao, J.; Kampf, J. W. Solid-State Packing of Conjugated Oligomers: From  $\pi$ -Stacks to the Herringbone Structure. *J. Am. Chem. Soc.* **2004**, *126* (13), 4318–4328.
- (40) Bondi, A. van der Waals Volumes and Radii. J. Phys. Chem. 1964, 68, 441-451.
- (41) Kreyes, A.; Mourran, A.; Hong, Z.; Wang, J.; Möller, M.; Gholamrezaie, F.; Roelofs, W. S. C.; de Leeuw, D. M.; Ziener, U. Predictability of Thermal and Electrical Properties of End-Capped Oligothiophenes by a Simple Bulkiness Parameter. *Chem. Mater.* **2013**, 25, 2128–2136.
- (42) Pensack, R. D.; Tilley, A. J.; Grieco, C.; Purdum, G. E.; Ostroumov, E. E.; Granger, D. B.; Oblinsky, D. G.; Dean, J. C.; Doucette, G. S.; Asbury, J. B.; Loo, Y.-L.; Seferos, D. S.; Anthony, J. E.; Scholes, G. D. Striking the right balance of intermolecular coupling for high-efficiency singlet fission. *Chem. Sci.* **2018**, *9*, 6240–6259.
- (43) Inoue, S.; Minemawari, H.; Tsutsumi, J. y.; Chikamatsu, M.; Yamada, T.; Horiuchi, S.; Tanaka, M.; Kumai, R.; Yoneya, M.; Hasegawa, T. Effects of Substituted Alkyl Chain Length on Solution-Processable Layered Organic Semiconductor Crystals. *Chem. Mater.* **2015**, 27, 3809–3812.